J. KSIAM Vol.10, No.1, 11-33, 2006

# MULTI-DIMENSIONAL LIMITING PROCESS FOR TWO-DIMENSIONAL COMPRESSIBLE FLOWS

Heeseok Koo, Sung-Hwan Yoon, Chongam Kim, and Kyu-Hong Kim

ABSTRACT Through the analysis of conventional TVD limiters, a new multi-dimensional limiting function is derived for an oscillation control in multi-dimensional flows. And, Multi-dimensional Limiting Process (MLP) is developed with the multi-dimensional limiting function. The major advantage of MLP is to prevent oscillations across a multi-dimensional discontinuity, and it is readily compatible with more than 3rd order spatial interpolation. Moreover, compared with other higher order interpolation schemes such as ENO-type schemes, MLP shows a good convergence characteristic in a steady problem and it is very simple to be implemented. In the present paper, 3rd and 5th order interpolation schemes with MLP, named MLP3 and MLP5, are developed and tested for several real applications, and it is verified that MLP combined with M-AUSMPW+ numerical flux substantially improves accuracy, efficiency and robustness both in continuous and discontinuous flows.

## 1. INTRODUCTION

At present stage, one of challenges in CFD is to provide an accurate and efficient solution in the analysis or design of three-dimensional aerodynamics. In order to cope with the requirement, a numerical scheme should be able to describe multi-dimensional flow phenomena as much as possible. However, up to now, most successful numerical methods, including spatial discretization and interpolation schemes, have been developed based on one-dimensional flow physics. Although this approach allows the rigorous analysis of numerical schemes, straightforward extension to two- or three-dimensional flows by dimensional splitting eventually leads to insufficient or excessive numerical dissipation, which in turn badly influences on the accuracy, robustness and convergence of numerical solutions. In other words, physically unacceptable interruption in numerics always results in the inaccurate representation of real physics.

In order to incorporate multi-dimensional physical phenomena, numerous approaches have been tried and developed by considering flow information along additional directions. Most

**AMS Subject Classification:**
**Key Words and Phrases:** Multi-dimensional limiting function, Multi-dimensional Limiting Process (MLP), Multi-dimensional flows, Entropy condition, Higher order spatial accuracy.

notably, by modeling wave-speeds [1], rotating fluxes at a cell-interface [2, 3, 4, 5], or by introducing fluctuation splitting and so on [6, 7, 8], various versions of multi-dimensional upwind fluxes have been developed. Obviously, a multi-dimensional scheme should bring noticeable improvement over conventional schemes in terms of accuracy. However, some degree of accuracy enhancement is compromised by robustness problem and computational cost, which is one of the obstacles in practical implementation. For example, most multi-dimensional schemes do not show monotonic behavior across a multi-dimensional discontinuity. When they are applied to high speed flow problems involving strong shocks, severe oscillations across strong shock are frequently generated and finally they may lead to a failure. One of the fundamental reasons, according to the authors' experience, is that there is not an appropriate oscillation control method for a pure multi-dimensional problem. Thus, it is important to develop an oscillation control process based on multi-dimensional flow phenomena.

Concerning oscillation control schemes, so many studies have been carried out since the late 1970s and several important concepts, such as TVD, TVB, ENO and etc, have been proposed for better convergence and stable calculation. The concept of TVD (Total Variation Diminishing) was proven to be extremely successful in solving hyperbolic conservation laws [9, 10]. Although TVD criterion provides fundamental idea for oscillation control and is still very popular, conventional TVD schemes are somewhat unsatisfactory near extrema in terms of accuracy and convergence. In order to overcome this limitation, ENO (Essentially Non-Oscillatory) schemes [11] and the concept of TVB (Total Variation Bounded) [12] were introduced. The key idea of ENO schemes is to use the smoothest stencil among several candidates in evaluating fluxes at a cell boundary which should yield higher order spatial accuracy and essential non-oscillatory profile near shocks. TVB concept allows oscillations only if spurious oscillations do not grow unboundedly large as time evolves. Although TVB or ENO avoids unphysical clipping at extrema and enhances accuracy, it is inevitable to yield undershoot and/or overshoot which in turn influences convergence badly. Most oscillation-free schemes have been based on the mathematical analysis of one-dimensional convection equation. Also, they are applied to multi-dimensional applications with dimensional splitting. Although they may work successfully in many cases, it is insufficient or almost impossible to control oscillations near shock discontinuity in multi-space dimensions. For that reason, the need of oscillation control method for multi-dimensional applications is obvious.

The objective of the present paper is to develop a higher order limiting process which can control oscillations in multi-dimensional situations and be applicable to both unsteady and steady problems. In this respect, convergence is an important factor. Firstly, we derive a multi-dimensional limiting function to control oscillations. For that purpose, we adopt TVD concept as a starting point since it shows a better convergence characteristic among available oscillation control methods. And, a higher order polynomial interpolation combined with the multi-dimensional limiting function, called Multi-dimensional Limiting Process (MLP), is developed which possesses a higher degree of accuracy, computational efficiency and convergence.

## 2. GOVERNING EQUATIONS

The two-dimensional Navier-Stokes equations in a conservative form is used as

$$\frac{\partial \mathbf{Q}}{\partial t}+\frac{\partial \mathbf{E}}{\partial x}+\frac{\partial \mathbf{F}}{\partial y}=\left(\frac{\partial \mathbf{E}_v}{\partial x}+\frac{\partial \mathbf{F}_v}{\partial y}\right), \tag{1}$$

where the flow and flux vectors are

$$\boldsymbol{Q}=\begin{pmatrix}\rho\\ \rho u\\ \rho v\\ \rho e_t\end{pmatrix}, \boldsymbol{E}=\begin{pmatrix}\rho u\\ \rho u^2+p\\ \rho uv\\ (\rho e_t+p)u\end{pmatrix}, \boldsymbol{F}=\begin{pmatrix}\rho v\\ \rho vu\\ \rho v^2+p\\ (\rho e_t+p)v\end{pmatrix}, \boldsymbol{E}_v=\begin{pmatrix}0\\ \tau_{xx}\\ \tau_{xy}\\ e_v\end{pmatrix}, \boldsymbol{F}_v=\begin{pmatrix}0\\ \tau_{xy}\\ \tau_{yy}\\ f_v\end{pmatrix}, \tag{2}$$

with $e_v=u\tau_{xx}+v\tau_{xy}-q_x$, $f_v=u\tau_{xy}+v\tau_{yy}-q_y$. For calorically perfect gas, the equation of state is given by

$$p=(\gamma-1)\rho e=(\gamma-1)\rho\left(e_t-\frac{1}{2}(u^2+v^2)\right), \tag{3}$$

with $\gamma=1.4$ for air.

## 3. MULTI-DIMENSIONAL LIMITING PROCESS (MLP)

### 3.1. High order TVD interpolation

MUSCL approach[15] – a method for the generation of second-order upwind schemes – with TVD limiter is written as follows.

$$\boldsymbol{\Phi}_L=\overline{\boldsymbol{\Phi}}_i+\frac{1}{4}\left[(1-\kappa)\phi(r_L)+(1+\kappa)r_L\phi\left(\frac{1}{r_L}\right)\right](\overline{\boldsymbol{\Phi}}_i-\overline{\boldsymbol{\Phi}}_{i-1}), \tag{4a}$$

$$\boldsymbol{\Phi}_R=\overline{\boldsymbol{\Phi}}_{i+1}-\frac{1}{4}\left[(1-\kappa)\phi(r_R)+(1+\kappa)r_R\phi\left(\frac{1}{r_R}\right)\right](\overline{\boldsymbol{\Phi}}_{i+2}-\overline{\boldsymbol{\Phi}}_{i+1}), \tag{4b}$$

where $\boldsymbol{\Phi}$ is a property vector, $r_L=\dfrac{\overline{\boldsymbol{\Phi}}_{i+1}-\overline{\boldsymbol{\Phi}}_i}{\overline{\boldsymbol{\Phi}}_i-\overline{\boldsymbol{\Phi}}_{i-1}}$ and $r_R=\dfrac{\overline{\boldsymbol{\Phi}}_{i+1}-\overline{\boldsymbol{\Phi}}_i}{\overline{\boldsymbol{\Phi}}_{i+2}-\overline{\boldsymbol{\Phi}}_{i+1}}$.

The bar means cell averaged value and $\phi$ is a TVD limiter which monitors the local gradient of property and determines local slope under monotonic condition. The calculated value has third order spatial accuracy with $\kappa=1/3$. As known well, if TVD limiter is symmetric, Eq.(4) is independent of $\kappa$ and simplified as follows.

$$\boldsymbol{\Phi}_L=\overline{\boldsymbol{\Phi}}_i+0.5\phi(r_L)(\overline{\boldsymbol{\Phi}}_i-\overline{\boldsymbol{\Phi}}_{i-1}), \tag{5a}$$

$$\boldsymbol{\Phi}_R=\overline{\boldsymbol{\Phi}}_{i+1}-0.5\phi(r_R)(\overline{\boldsymbol{\Phi}}_{i+2}-\overline{\boldsymbol{\Phi}}_{i+1}), \tag{5b}$$

where $\phi(r) = r\phi(1/r)$.

In flows including physical discontinuities, $\phi$ is definitely employed to yield monotonic distribution. Equations (6) to (8) show well-known existing TVD limiters.

Minmod limiter : $$\phi(r) = \max(0, \min(r,1)). \tag{6}$$

Van Leer limiter: $$\phi(r) = \frac{r + |r|}{1 + |r|}. \tag{7}$$

Superbee limiter: $$\phi(r) = \max(0, \min(2r,1), \min(r,2)). \tag{8}$$

Interpolation step is generally considered to be independent of flow physics and only related to mathematics. Thus, up to now, the entropy condition has been considered only at evaluation stage. However, if we use the same limiter both in isentropic compression and isentropic expansion flows, one of cases definitely brings negative entropy variation at interpolation step. In many applications, negative entropy variation is not amplified and makes no serious problem. However, it can not be guaranteed in cases involving strong expansion. Therefore, flow physics such as the entropy condition is critical both at evolution stage and at interpolation stage.

When 2nd order MUSCL approach is applied, there is no concrete information on the variation of $\Delta\Phi_{optimal}\big|_i$, except for the monotonic constraint of $\min(\Delta\Phi_{i-\frac{1}{2}}, \Delta\Phi_{i+\frac{1}{2}}) < \Delta\Phi_{optimal}\big|_i < \max(\Delta\Phi_{i-\frac{1}{2}}, \Delta\Phi_{i+\frac{1}{2}})$. Therefore, it is intrinsically problematic in the 2nd order interpolation schemes. Let optimal variation be $\Delta\Phi_{optimal}\big|_i = \beta\Delta\Phi_{i-\frac{1}{2}}$, where $\beta$ has to be specified. Improper choice of $\beta$ would yield dissipative or entropy-violating result as in case of minmod or superbee limiter. In order to determine $\beta$ based on flow physics, more than 3rd order spatial interpolation is essential because the second order interpolation cannot reflect the curvature of $\Phi$.

### 3.1.1 3rd order interpolation with TVD limiting:

Similar to reconstruction by the primitive function in ENO [11], 3rd order interpolation which satisfies the conservation requirement is applied. For equally spacing grid points, $\Phi$ is given by

$$\Phi(x) = ax^2 + bx + c. \tag{9}$$

And, the cell-averaged value is (see Fig. 1)

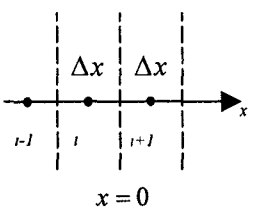


Fig.1 Cell center point and cell-interface

$$\frac{1}{\Delta x}\int_{(m-1)\Delta x}^{m\Delta x}\Phi(x)dx=\overline{\Phi}_{i+m}\ \ (m=-1,0,1). \tag{10}$$

Then, from Eqs.(9) and (10), the value of $\Phi$ at a cell-interface is written as,

$$\Phi_{i+\frac{1}{2}}=\frac{2\overline{\Phi}_{i+1}+5\overline{\Phi}_{i}-\overline{\Phi}_{i-1}}{6}=\overline{\Phi}_{i}+0.5\frac{\Delta\Phi_{i-\frac{1}{2}}+2\Delta\Phi_{i+\frac{1}{2}}}{3}=\overline{\Phi}_{i}+0.5\beta(r_i)\Delta\Phi_{i-\frac{1}{2}}, \tag{11}$$

where $\beta=\frac{1+2r_i}{3}$ and $r_i=\frac{\Delta\Phi_{i+\frac{1}{2}}}{\Delta\Phi_{i-\frac{1}{2}}}$.

To suppress oscillations across a discontinuity, TVD limiting condition of $\max(0,\min(2,2r))$ is applied to Eq.(11) [10]. Then, the higher order interpolation filtered by TVD limiting can be written as $\phi(r)=\max(0,\min(2,2r,\beta))$. Finally, left and right cell-interface values are obtained as follows.

$$\Phi_L=\overline{\Phi}_{i}+0.5\phi(r_{L,i})\Delta\Phi_{i-\frac{1}{2}}=\overline{\Phi}_{i}+0.5\max(0,\min(2,2r_{L,i},\beta_L))\Delta\Phi_{i-\frac{1}{2}}, \tag{12a}$$

$$\Phi_R=\overline{\Phi}_{i+1}-0.5\phi(r_{R,i+1})\Delta\Phi_{i+\frac{3}{2}}=\overline{\Phi}_{i+1}-0.5\max(0,\min(2,2r_{R,i+1},\beta_R))\Delta\Phi_{i+\frac{3}{2}}. \tag{12b}$$

In Eq.(12), $\beta_L$ and $\beta_R$ are given as follows.

$$\beta_L=\frac{1+2r_{L,i}}{3},\ \ \beta_R=\frac{1+2r_{R,i+1}}{3},\ \text{with}\ \ r_{L,i}=\frac{\Delta\Phi_{i+\frac{1}{2}}}{\Delta\Phi_{i-\frac{1}{2}}}\ \ \ r_{R,i+1}=\frac{\Delta\Phi_{i+\frac{1}{2}}}{\Delta\Phi_{i+\frac{3}{2}}}. \tag{13}$$

### 3.1.2 5th order interpolation with TVD limiting:

In a similar way, 5th order interpolation can be obtained as $\Phi(x)=ax^4+bx^3+cx^2+dx+e$. And, the interpolated value $\Phi$ at a cell-interface is given by

$$\begin{aligned}\Phi_{i+\frac{1}{2}}&=\frac{2\overline{\Phi}_{i-2}-13\overline{\Phi}_{i-1}+47\overline{\Phi}_{i}+27\overline{\Phi}_{i+1}-3\overline{\Phi}_{i+2}}{60}\\&=\overline{\Phi}_{i}+0.5\frac{-2\Delta\Phi_{i-\frac{3}{2}}+11\Delta\Phi_{i-\frac{1}{2}}+24\Delta\Phi_{i+\frac{1}{2}}-3\Delta\Phi_{i+\frac{3}{2}}}{30},\\&=\overline{\Phi}_{i}+0.5\beta(r_{i-1},r_i,r_{i+1})\Delta\Phi_{i-\frac{1}{2}}\end{aligned} \tag{14}$$

where $\beta=\frac{-2/r_{i-1}+11+24r_i-3r_ir_{i+1}}{30}$, $r_{i-1}=\frac{\Delta\Phi_{i-\frac{1}{2}}}{\Delta\Phi_{i-\frac{3}{2}}}$, $r_i=\frac{\Delta\Phi_{i+\frac{1}{2}}}{\Delta\Phi_{i-\frac{1}{2}}}$ and $r_{i+1}=\frac{\Delta\Phi_{i+\frac{3}{2}}}{\Delta\Phi_{i+\frac{1}{2}}}$. It is noted that $\beta$ of 5th order interpolation is the function of $r_{i-1}$, $r_i$ and $r_{i+1}$. Finally, the fifth order interpolation scheme filtered by TVD limiting can be written as follows.

$$\Phi_L=\overline{\Phi}_{i}+0.5\phi(r_L)\Delta\Phi_{i-\frac{1}{2}}=\overline{\Phi}_{i}+0.5\max(0,\min(2,2r_{L,i},\beta_L))\Delta\Phi_{i-\frac{1}{2}}, \tag{15a}$$

$$\Phi_R=\overline{\Phi}_{i+1}-0.5\phi(r_R)\Delta\Phi_{i+\frac{3}{2}}=\overline{\Phi}_{i+1}-0.5\max(0,\min(2,2r_{R,i+1},\beta_R))\Delta\Phi_{i+\frac{3}{2}}. \tag{15b}$$

In Eq.(15), $\beta_L$ and $\beta_R$ is given as follows.

$$\beta_L = \frac{-2/r_{L,I-1} + 11 + 24r_{L,I} - 3r_{L,I}r_{L,I+1}}{30}, \quad \beta_R = \frac{-2/r_{R,I+2} + 11 + 24r_{R,I+1} - 3r_{R,I+1}r_{R,I}}{30}, \tag{16}$$

where $r_{L,I-1} = \frac{\Delta\Phi_{I-\frac{1}{2}}}{\Delta\Phi_{I-\frac{3}{2}}}$, $r_{L,I} = \frac{\Delta\Phi_{I+\frac{1}{2}}}{\Delta\Phi_{I-\frac{1}{2}}}$, $r_{L,I+1} = \frac{\Delta\Phi_{I+\frac{3}{2}}}{\Delta\Phi_{I+\frac{1}{2}}}$ and $r_{R,I+2} = \frac{\Delta\Phi_{I+\frac{3}{2}}}{\Delta\Phi_{I+\frac{5}{2}}}$, $r_{R,I+1} = \frac{\Delta\Phi_{I+\frac{1}{2}}}{\Delta\Phi_{I+\frac{3}{2}}}$, $r_{R,I} = \frac{\Delta\Phi_{I-\frac{1}{2}}}{\Delta\Phi_{I+\frac{1}{2}}}$.

### 3.2 Development of Multi-dimensional Limiting Process (MLP)

Since the late 1970s, numerous ways to control oscillations have been studied and several limiting concepts have been proposed. Most representatives would be TVD, TVB and ENO. In case of scalar convection equation, rigorous mathematical analysis unveils their good characteristics. However, it looks very difficult to prove similar behaviors in non-linear systems of equations. Thus, the successful application of these approaches to multi-dimensional systems is largely based on some linearization step and some practical experience. Even though they can be applied successfully in many cases, some weakness is still observed in calculating shock discontinuity in multi-dimensional flow. Therefore, it is believed that the previous limiting concept based on one-dimensional flow physics has to be improved and a new limiting process has to be introduced based on multi-dimensional flow physics.

One of the fundamental difficulties in handling multi-dimensional problems is that it is difficult to define monotonic characteristic [16] and especially, the definition of monotonic distribution is ambiguous near a saddle point. In addition, Goodman and LeVeque showed TVD scheme in two space dimensions can not be more than first order accurate [17]. Thus, it looks nearly impossible to develop an oscillation control scheme with global higher order accuracy in multi-space dimensions. However, if we focus on more specific issue, the limitation of the previous oscillation control concept can be improved. For that reason, Spekreijse defined his own version of multi-dimensional monotonic condition, and derived a second order monotone upwind scheme which satisfies his multi-dimensional monotonic condition in steady case. The monotone scheme was analyzed based on a non-linear scalar equation [18]. Although it shows good performances in scalar convection equation, it does not seem to be good enough to control oscillations in multi-dimensional shock discontinuity and requires some unknown parameter.

In the present paper, we mainly focus on oscillation control across a multi-dimensional shock discontinuity to sidestep the difficulty in defining multi-dimensional monotonic distribution exactly. Then, a multi-dimensional limiting function is derived using nine point stencil as in Fig.2. It is based on oscillation control concept because this is more flexible to deal with multi-dimensional situation than strict monotonic concept. TVD is adopted for that purpose.

#### 3.2.1 Derivation of a multi-dimensional limiting function

One-dimensional limiting condition using TVD constraint can be written as follows [10].

$$0 \le \phi(r) \le \min(2r, 2). \tag{17}$$

Since the extension of Eq.(17) in a dimensional splitting manner is insufficient to prevent oscillations in multi-dimensional flow, it needs to be modified and/or extended with appropriate consideration of multi-dimensional situation. From Eq.(17) and Eq.(5), the property at a cell-interface satisfies $\overline{\Phi}_{i-1} \le \Phi_{i-\frac{1}{2}} \le \overline{\Phi}_i$ and $\overline{\Phi}_i \le \Phi_{i+\frac{1}{2}} \le \overline{\Phi}_{i+1}$. Thus, the dimensional splitting extension of this distribution is

$$\overline{\Phi}_{i-1,j} \le \Phi_{i-\frac{1}{2},j} \le \overline{\Phi}_{i,j}, \quad \overline{\Phi}_{i,j} \le \Phi_{i+\frac{1}{2},j} \le \overline{\Phi}_{i+1,j}, \quad \overline{\Phi}_{i,j-1} \le \Phi_{i,j-\frac{1}{2}} \le \overline{\Phi}_{i,j}, \quad \overline{\Phi}_{i,j} \le \Phi_{i,j+\frac{1}{2}} \le \overline{\Phi}_{i,j+1}. \tag{18}$$

It is noted that Eq.(18) does not possess any information on the property distribution at cell vertex points, which would be essential when property gradient is not aligned with grid lines. Thus, as an extended condition of Eq.(18) which includes the missing information, we require Eq.(19) on compact stencil in Fig.3.

$$\overline{\Phi}^{\min}_{neighbor} < \Phi < \overline{\Phi}^{\max}_{neighbor}. \tag{19}$$

Since Eq.(17) does not automatically imply Eq.(19), Eq.(17) as well as Eq.(19) has to be satisfied to control oscillations in multi-space dimensions. In order to realize Eq.(19), the values at vertex points, $\Phi_1$, $\Phi_2$, $\Phi_3$ and $\Phi_4$ in Fig.3, are required to satisfy

$$\min\left(\overline{\Phi}_{i,j}, \overline{\Phi}_{i+1,j}, \overline{\Phi}_{i,j-1}, \overline{\Phi}_{i+1,j-1}\right) < \Phi_1 < \max\left(\overline{\Phi}_{i,j}, \overline{\Phi}_{i+1,j}, \overline{\Phi}_{i,j-1}, \overline{\Phi}_{i+1,j-1}\right), \tag{20a}$$

$$\min\left(\overline{\Phi}_{i,j}, \overline{\Phi}_{i+1,j}, \overline{\Phi}_{i,j+1}, \overline{\Phi}_{i+1,j+1}\right) < \Phi_2 < \max\left(\overline{\Phi}_{i,j}, \overline{\Phi}_{i+1,j}, \overline{\Phi}_{i,j+1}, \overline{\Phi}_{i+1,j+1}\right), \tag{20b}$$

$$\min\left(\overline{\Phi}_{i,j}, \overline{\Phi}_{i-1,j}, \overline{\Phi}_{i,j+1}, \overline{\Phi}_{i-1,j+1}\right) < \Phi_3 < \max\left(\overline{\Phi}_{i,j}, \overline{\Phi}_{i-1,j}, \overline{\Phi}_{i,j+1}, \overline{\Phi}_{i-1,j+1}\right), \tag{20c}$$

$$\min\left(\overline{\Phi}_{i,j}, \overline{\Phi}_{i-1,j}, \overline{\Phi}_{i,j-1}, \overline{\Phi}_{i-1,j-1}\right) < \Phi_4 < \max\left(\overline{\Phi}_{i,j}, \overline{\Phi}_{i-1,j}, \overline{\Phi}_{i,j-1}, \overline{\Phi}_{i-1,j-1}\right). \tag{20d}$$

And, a multi-dimensional limiting function which is compatible with Eq.(17) and at the same time yield the distribution of Eq.(20) has to be formulated.

If discontinuity is inclined by $\theta_j$ as in Fig.3 and $0 < \theta_j < 90^\circ$, Eq.(20) becomes

$$\overline{\Phi}_{i,j-1} < \Phi_1 < \overline{\Phi}_{i+1,j}, \tag{21a}$$

$$\overline{\Phi}_{i,j} < \Phi_2 < \overline{\Phi}_{i+1,j+1}, \tag{21b}$$

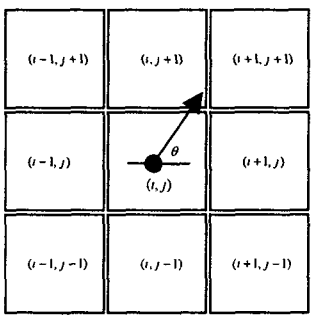


Fig. 2 Neighboring cells to derive the multi-dimensional limiting function

$$\overline{\Phi}_{i-1,j} < \Phi_3 < \overline{\Phi}_{i,j+1}, \tag{21c}$$
$$\overline{\Phi}_{i-1,j-1} < \Phi_4 < \overline{\Phi}_{i,j}. \tag{21d}$$

The case of $90^\circ < \theta_j < 180^\circ$ is symmetric with respect to $\eta = 0$ line, the case of $180^\circ < \theta_j < 270^\circ$ is the same as the case of $0^\circ < \theta_j < 90^\circ$ and the case of $270^\circ < \theta_j < 360^\circ$ is symmetric with respect to $\xi = 0$ line. Now, let us consider the values at four vertex points which are evaluated as

$$\Phi_1 = \overline{\Phi}_{i,j} + \Delta\Phi_\eta^- + \Delta\Phi_\xi^+, \tag{22a}$$
$$\Phi_2 = \overline{\Phi}_{i,j} + \Delta\Phi_\eta^+ + \Delta\Phi_\xi^+ = \overline{\Phi}_{i,j} + \left(1 + \tan\tilde{\theta}_j\right)\Delta\Phi_\eta^+, \tag{22b}$$
$$\Phi_3 = \overline{\Phi}_{i,j} + \Delta\Phi_\eta^+ + \Delta\Phi_\xi^-, \tag{22c}$$
$$\Phi_4 = \overline{\Phi}_{i,j} + \Delta\Phi_\eta^- + \Delta\Phi_\xi^- = \overline{\Phi}_{i,j} + \left(1 + \tan\tilde{\theta}_j\right)\Delta\Phi_\eta^-, \tag{22d}$$

where $\tilde{\theta}$ is defined as $\tan\tilde{\theta}_j = \dfrac{\Delta\Phi_\xi^+}{\Delta\Phi_\eta^+}$ in Fig.3. $\Delta\Phi_{\xi,\eta}^{\pm}$ are the variations from center point to cell-interface as in Fig.4. Thus, $\Delta\Phi^{\pm}$ has an opposite sign with each other: when $0 < \theta_j < 90^\circ$, $\Delta\Phi^+$ is positive and $\Delta\Phi^-$ is negative and $\tan\tilde{\theta} > 0$.

From Eq.(18), the interpolated value $\Phi_{i,j\pm\frac{1}{2}}$ and $\Phi_{i\pm\frac{1}{2},j}$ should satisfy the following conditions.

$$\overline{\Phi}_{i-1,j} \le \Phi_{i-\frac{1}{2},j} \le \overline{\Phi}_{i,j} \le \Phi_{i+\frac{1}{2},j} \le \overline{\Phi}_{i+1,j}, \tag{23a}$$
$$\overline{\Phi}_{i,j-1} \le \Phi_{i,j-\frac{1}{2}} \le \overline{\Phi}_{i,j} \le \Phi_{i,j+\frac{1}{2}} \le \overline{\Phi}_{i,j+1}, \tag{23b}$$

where $\Phi_{i\pm\frac{1}{2},j} = \overline{\Phi}_{i,j} + \Delta\Phi_\xi^{\pm}$ and $\Phi_{i,j\pm\frac{1}{2}} = \overline{\Phi}_{i,j} + \Delta\Phi_\eta^{\pm}$. From Eqs.(22) and (23), $\Phi_1$ is always greater than $\overline{\Phi}_{i,j-1}$ and less than $\overline{\Phi}_{i+1,j}$ because $\Delta\Phi^+$ is positive and $\Delta\Phi^-$ is negative. Similarly, $\Phi_3$ is always greater than $\overline{\Phi}_{i-1,j}$ and less than $\overline{\Phi}_{i,j+1}$.

$$\overline{\Phi}_{i,j-1} < \Phi_{i,j-\frac{1}{2}} < \overline{\Phi}_{i,j} + \Delta\Phi_\eta^- + \Delta\Phi_\xi^+ = \Phi_1 < \Phi_{i+\frac{1}{2},j} < \overline{\Phi}_{i+1,j}, \tag{24a}$$
$$\overline{\Phi}_{i-1,j} < \Phi_{i-\frac{1}{2},j} < \overline{\Phi}_{i,j} + \Delta\Phi_\xi^- + \Delta\Phi_\eta^+ = \Phi_3 < \Phi_{i,j+\frac{1}{2}} < \overline{\Phi}_{i,j+1}. \tag{24b}$$

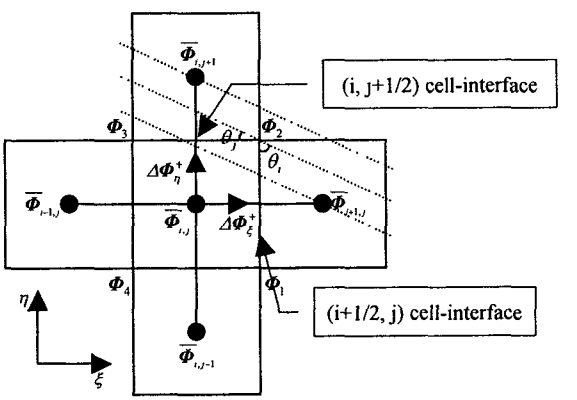


Fig.3 Distributions of cell averaged values and cell vertex values

Thus, $\Phi_1$ and $\Phi_3$ always satisfy Eqs.(21a) and (21c). Now, let us check the cases of $\Phi_2$ and $\Phi_4$. In case of $\Phi_2$, from $\overline{\Phi}_{i,j} < \Phi_2 = \overline{\Phi}_{i,j} + \left(1+\tan\tilde{\theta}_j\right)\Delta\Phi_\eta^+$, Eq.(21b) is satisfied only if $\Phi_2$ would be less than $\overline{\Phi}_{i+1,j+1}$.

$$\Phi_2 = \overline{\Phi}_{i,j} + \left(1+\tan\tilde{\theta}_j\right)\Delta\Phi_\eta^+ \le \overline{\Phi}_{i+1,j+1} = \overline{\Phi}_{i,j} + \Delta\Phi_{i,j+\frac{1}{2}} + \Delta\Phi_{i+\frac{1}{2},j+1}. \tag{25}$$

$$\Delta\Phi_{i+\frac{1}{2},j+1} = \tan\bar{\theta}_{j+1}\Delta\Phi_{i,j+\frac{3}{2}} = \tan\bar{\theta}_{j+1}\frac{\Delta\Phi_{i,j+\frac{3}{2}}}{\Delta\Phi_{i,j+\frac{1}{2}}}\Delta\Phi_{i,j+\frac{1}{2}} = \frac{\tan\bar{\theta}_{j+1}}{r_{R,j+1}}\Delta\Phi_{i,j+\frac{1}{2}}, \tag{26}$$

where $\bar{\theta}$ is defined as $\tan\bar{\theta}_{j+1} = \dfrac{\Delta\Phi_{i+\frac{1}{2},j+1}}{\Delta\Phi_{i,j+\frac{3}{2}}}$ and $r_{R,j+1} = \dfrac{\Delta\Phi_{i,j+\frac{1}{2}}}{\Delta\Phi_{i,j+\frac{3}{2}}}$. Thus, from Eqs.(25) and (26),

$$\Delta\Phi_\eta^+ \le \frac{\left(1+\dfrac{\tan\bar{\theta}_{j+1}}{r_{R,j+1}}\right)}{\left(1+\tan\tilde{\theta}_j\right)}\Delta\Phi_{i,j+\frac{1}{2}}. \tag{27}$$

And, from Eqs.(5) and (17), the maximum variation of $\Delta\Phi_\eta^+$ is determined as

$$\Delta\Phi_\eta^+ = \Delta\Phi_{i,j-\frac{1}{2}} \quad (r_{L,j} > 1), \qquad \Delta\Phi_\eta^+ = \Delta\Phi_{i,j+\frac{1}{2}} \quad (0 < r_{L,j} < 1), \tag{28}$$

where $r_{L,j} = \dfrac{1}{r_{R,j}} = \dfrac{\Delta\Phi_{i,j+\frac{1}{2}}}{\Delta\Phi_{i,j-\frac{1}{2}}}$. Thus, by limiting the maximum variation of $\Delta\Phi_\eta^+$, all of the Eqs.(21) can be realized as follows.

When $r_{L,j} > 1$,

The maximum variation is modified as $\Delta\Phi_\eta^+ = 0.5\alpha\Delta\Phi_{i,j-\frac{1}{2}}$ instead of $\Delta\Phi_\eta^+ = \Delta\Phi_{i,j-\frac{1}{2}}$. Then, from Eq.(27), we can determine the value of $\alpha$ $(1 \le \alpha \le 2)$ which satisfies Eq.(24b).

$$0.5\frac{\alpha}{r_{L,j}}\Delta\Phi_{i,j+\frac{1}{2}} \le \frac{\left(1+\dfrac{\tan\bar{\theta}_{j+1}}{r_{R,j+1}}\right)}{\left(1+\tan\tilde{\theta}_j\right)}\Delta\Phi_{i,j+\frac{1}{2}}, \tag{29a}$$

where $\Delta\Phi_\eta^+ = 0.5\alpha\Delta\Phi_{i,j-\frac{1}{2}} = 0.5\dfrac{\alpha}{r_{L,j}}\Delta\Phi_{i,j+\frac{1}{2}}$ $(1 \le \alpha \le 2)$. Thus, we have

$$1 \le \alpha \le \min\left[2, \frac{2r_{L,j}\left(1+\dfrac{\tan\bar{\theta}_{j+1}}{r_{R,j+1}}\right)}{\left(1+\tan\tilde{\theta}_j\right)}\right]. \tag{29b}$$

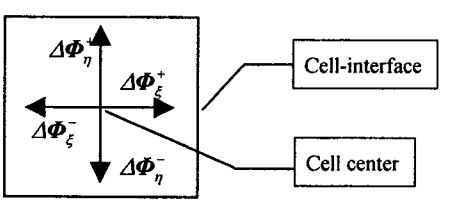


Fig. 4 Definition of property variations within a cell

When $0 < r_{L,J} < 1$,

Similarly, the maximum variation is modified as $\Delta\Phi_{\eta}^{+} = 0.5\alpha\Delta\Phi_{i,J+\frac{1}{2}}$ instead of $\Delta\Phi_{\eta}^{+} = \Delta\Phi_{i,J+\frac{1}{2}}$. By inserting $\Delta\Phi_{\eta}^{+} \le 0.5\alpha\Delta\Phi_{i,J+\frac{1}{2}}$ $(1 \le \alpha \le 2)$ into Eq.(27),

$$0.5\alpha\Delta\Phi_{i,J+\frac{1}{2}} \le \frac{\left(1+\dfrac{\tan\bar{\theta}_{J+1}}{r_{R,J+1}}\right)}{\left(1+\tan\tilde{\theta}_{J}\right)}\Delta\Phi_{i,J+\frac{1}{2}} \tag{30a}$$

Then, we obtain

$$1 \le \alpha \le \min\left[2, \frac{2\left(1+\dfrac{\tan\bar{\theta}_{J+1}}{r_{R,J+1}}\right)}{\left(1+\tan\tilde{\theta}_{J}\right)}\right]. \tag{30b}$$

Equations (29b) and (30b) always make $\Phi_2$ less than $\bar{\Phi}_{i+1,J+1}$, and Eq.(21b) is realized.

Next, let us consider the case of $r_{R,J+1} < 0$ in Eq. (27). From Eq.(26), it is the case where $\bar{\Phi}_{i+1,J+1}$ is less than $\bar{\Phi}_{i,J+1}$. If the case of $r_{R,J+1} < 0$ is ignored, $\alpha$ is restricted too much and a computed solution can be undesirably diffusive. Thus, the condition, that $\Phi_2$ should be less than $\bar{\Phi}_{i,J+1}$ instead of $\bar{\Phi}_{i+1,J+1}$ when $r_{R,J+1} < 0$, is introduced. When $r_{R,J+1} < 0$, we require

$$\Phi_2 = \bar{\Phi}_{i,J} + \left(1+\tan\tilde{\theta}_{j}\right)\Delta\Phi_{\eta}^{+} \le \bar{\Phi}_{i,J+1} = \bar{\Phi}_{i,J} + \Delta\Phi_{i,J+\frac{1}{2}}. \tag{31a}$$

Then,

$$\Delta\Phi_{\eta}^{+} \le \frac{1}{\left(1+\tan\tilde{\theta}_{J}\right)}\Delta\Phi_{i,J+\frac{1}{2}}. \tag{31b}$$

Similar to the above procedure, the range of the restriction coefficient $\alpha$ is derived for the following cases.

When $r_{L,J} > 1$ and $r_{R,J+1} < 0$,

$$1 \le \alpha \le \min\left[2, \frac{2r_{L,J}}{\left(1+\tan\tilde{\theta}_{J}\right)}\right]. \tag{32}$$

When $0 < r_{L,J} < 1$ and $r_{R,J+1} < 0$,

$$1 \le \alpha \le \frac{2}{\left(1+\tan\tilde{\theta}_{J}\right)}. \tag{33}$$

Finally, by combining Eqs. (29b), (30b), (32) and (33), the range of $\alpha$ can be formulated as follows.

$$1 \le \alpha \le \min\left[2, \frac{2\max\left(1, r_{L,J}\right)\left(1+\max\left(0, \dfrac{\tan\bar{\theta}_{J+1}}{r_{R,J+1}}\right)\right)}{\left(1+\tan\tilde{\theta}_{J}\right)}\right]. \tag{34}$$

Equation (34) expresses the information of the restriction coefficient $\alpha$ for multi-dimensional monotonicity. If we choose the maximum value of $\alpha$, the multi-dimensional limiting function is obtained as follows.

The value of $\alpha$ contains two angles related to property variation, $\tilde{\theta}$ and $\bar{\theta}$, defined at each cell. Although $\tilde{\theta}$ and $\bar{\theta}$ are defined separately for the purpose of rigor, the difference is negligible in real computations, which will be shown well through test problems in Section 4. Thus, for computational efficiency we introduce the representative angle, $\theta$. It can be reasonably assumed that the three angles ( $\tilde{\theta}$, $\bar{\theta}$, $\theta$) are the same. From the definition of $\tilde{\theta}$ and $\bar{\theta}$,

$$\tan\tilde{\theta}_j = \frac{\Delta\Phi^+_\xi}{\Delta\Phi^+_\eta} \quad \text{and} \quad \tan\bar{\theta}_j = \frac{\Delta\Phi_{i+\frac{1}{2},j}}{\Delta\Phi_{i,j+\frac{1}{2}}}, \tag{35}$$

where $0^\circ < \theta_j < 90^\circ$. These are simply the ratios of variations in the $\xi$ and $\eta$ directions defined at each cell. Similarly, we define the following representative ratio of variation as

$$\tan\theta_j = \frac{\left(\overline{\Phi}_{i+1,j} - \overline{\Phi}_{i-1,j}\right)}{\left(\overline{\Phi}_{i,j+1} - \overline{\Phi}_{i,j-1}\right)} > 0. \tag{36}$$

Figures 5 show the definitions of three angles. When $90^\circ < \theta_j < 180^\circ$, the maximum value is $\overline{\Phi}_{i-1,j+1}$ in Fig. 3 with $\Delta\Phi^-_\xi > 0$, $\Delta\Phi^+_\eta > 0$. Thus,

$$\tan\tilde{\theta}_j = \frac{\Delta\Phi^-_\xi}{\Delta\Phi^+_\eta} > 0. \tag{37}$$

In this case, $\tan\theta_j$ is written as follows.

$$\tan\theta_j = -\frac{\left(\overline{\Phi}_{i+1,j} - \overline{\Phi}_{i-1,j}\right)}{\left(\overline{\Phi}_{i,j+1} - \overline{\Phi}_{i,j-1}\right)} > 0. \tag{38}$$

The cases of $180^\circ < \theta_j < 270^\circ$ and $270^\circ < \theta_j < 360^\circ$ can be handled in the same way. Finally, we have the following expression for the representative angle

$$\tan\theta_j = \left|\frac{\left(\overline{\Phi}_{i+1,j} - \overline{\Phi}_{i-1,j}\right)}{\left(\overline{\Phi}_{i,j+1} - \overline{\Phi}_{i,j-1}\right)}\right|. \tag{39}$$

As a consequence, the one-dimensional limiting condition and the multi-dimensional limiting function are compared as follows.

*One-dimensional limiting condition:* $\max(0,\min(2r,2))$. (40)

*Multi-dimensional limiting function:* $\max(0,\min(\alpha r,\alpha))$. (41)

$\Phi_4$ requires the same condition.

### 3.2.2 General form of Multi-dimensional Limiting Process (MLP)

With the multi-dimensional limiting function of Eq.(41), a new family of interpolation scheme to control oscillations in a multi-dimensional flow can be developed.

$$\Phi_L = \overline{\Phi}_i + 0.5\phi(r_{L,i},\alpha_L,\beta_L)\Delta\Phi_{i-\frac{1}{2}} = \overline{\Phi}_i + 0.5\max(0,\min(\alpha_L r_{L,i},\alpha_L,\beta_L))\Delta\Phi_{i-\frac{1}{2}}, \tag{42a}$$

$$\boldsymbol{\Phi}_R = \overline{\boldsymbol{\Phi}}_{i+1} - 0.5\phi(r_{R,i+1}, \alpha_R, \beta_R)\Delta\boldsymbol{\Phi}_{i+\frac{3}{2}} = \overline{\boldsymbol{\Phi}}_{i+1} - 0.5\max(0, \min(\alpha_R r_{R,i+1}, \alpha_R, \beta_R))\Delta\boldsymbol{\Phi}_{i+\frac{3}{2}}. \tag{42b}$$

The interpolated values of $\boldsymbol{\Phi}_L$ and $\boldsymbol{\Phi}_R$ are based on the final form of MLP. By inserting Eqs.(42) into Eqs.(31) and (23) in [14], MLP combined with M-AUSMPW+ are constructed. Other numerical flux can be employed similarly.

Values of $\alpha_{L,R}$ and $\beta_{L,R}$ in Eq.(42) is summarized as follows.

Along the $\xi$-direction,

$$\alpha_L = g\left[\frac{2\max(1, r_{L,i})\left(1+\max\left(0, \frac{\tan\theta_{i+1}}{r_{R,i+1}}\right)\right)}{1+\tan\theta_i}\right], \quad \alpha_R = g\left[\frac{2\max(1, r_{R,i+1})\left(1+\max\left(0, \frac{\tan\theta_i}{r_{L,i}}\right)\right)}{1+\tan\theta_{i+1}}\right], \tag{43a}$$

where $r_{L,i} = \dfrac{\Delta\boldsymbol{\Phi}_{i+\frac{1}{2},j}}{\Delta\boldsymbol{\Phi}_{i-\frac{1}{2},j}}$, $r_{R,i+1} = \dfrac{\Delta\boldsymbol{\Phi}_{i+\frac{1}{2},j}}{\Delta\boldsymbol{\Phi}_{i+\frac{3}{2},j}}$ and $g(x) = \max(1, \min(2, x))$.

Along the $\eta$-direction,

$$\alpha_L = g\left[\frac{2\max(1, r_{L,j})\left(1+\max\left(0, \frac{\tan\theta_{j+1}}{r_{R,j+1}}\right)\right)}{1+\tan\theta_j}\right], \quad \alpha_R = g\left[\frac{2\max(1, r_{R,j+1})\left(1+\max\left(0, \frac{\tan\theta_j}{r_{L,j}}\right)\right)}{1+\tan\theta_{j+1}}\right], \tag{43b}$$

where $r_{L,j} = \dfrac{\Delta\boldsymbol{\Phi}_{i,j+\frac{1}{2}}}{\Delta\boldsymbol{\Phi}_{i,j-\frac{1}{2}}}$, $r_{R,j+1} = \dfrac{\Delta\boldsymbol{\Phi}_{i,j+\frac{1}{2}}}{\Delta\boldsymbol{\Phi}_{i,j+\frac{3}{2}}}$, $\tan\theta_i = \left|\dfrac{\left(\overline{\boldsymbol{\Phi}}_{i,j+1} - \overline{\boldsymbol{\Phi}}_{i,j-1}\right)}{\left(\overline{\boldsymbol{\Phi}}_{i+1,j} - \overline{\boldsymbol{\Phi}}_{i-1,j}\right)}\right|$, $\tan\theta_j = \left|\dfrac{\left(\overline{\boldsymbol{\Phi}}_{i+1,j} - \overline{\boldsymbol{\Phi}}_{i-1,j}\right)}{\left(\overline{\boldsymbol{\Phi}}_{i,j+1} - \overline{\boldsymbol{\Phi}}_{i,j-1}\right)}\right|$.

Combining Eqs.(42) and (43) with Eqs.(13) and (15) for $\beta$, we finally obtain MLP3, MLP5.

*MLP with $3^{rd}$ order interpolation (MLP3):*

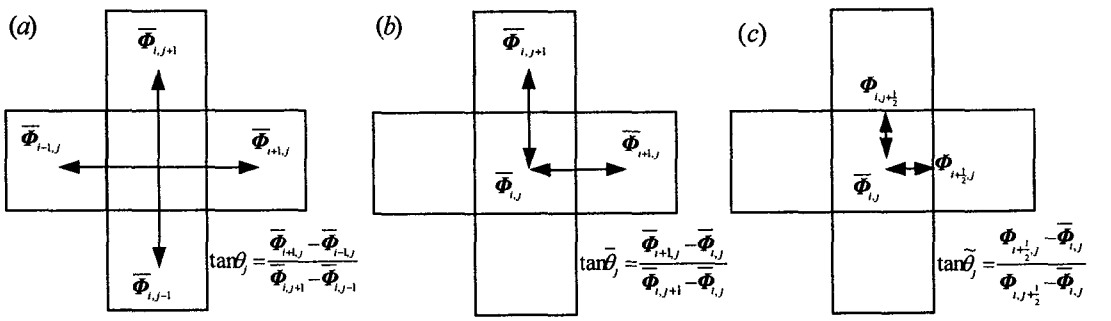


Fig.5 Definition of three angles

$$\beta_L = \frac{1+2r_{L,i}}{3}, \quad \beta_R = \frac{1+2r_{R,i+1}}{3}. \tag{44a}$$

*MLP with 5$^{th}$ order interpolation (MLP5):*

$$\beta_L = \frac{-2/r_{L,i-1}+11+24r_{L,i}-3r_{L,i}r_{L,i+1}}{30}, \quad \beta_R = \frac{-2/r_{R,i+2}+14+24r_{R,i+1}-3r_{R,i+1}r_{R,i}}{30}. \tag{44b}$$

### 3.3. Comparison between MLP and TVD limiters

To compare MLP with several TVD limiters, all of the limiters are re-written by the $\beta$ parameter form as

$$\phi = \max(0, \min(\beta_1 r, 1), \min(r, \beta_2)), \quad 1 < \beta_1, \beta_2 < 2. \tag{45}$$

Let us assume some interpolation function $f(r)$ is given within second order TVD region. When $0 < r < 1$, $f(r)$ should be within the region A in Fig.6, that is, $r < f(r) < 2r$ and $f(r) < 1$. In the $\beta$ limiter form, it corresponds to

$$\phi = \max(0, \min(\beta_1 r, 1), r) = \min(\beta_1 r, 1), \quad \beta_1 = \min\left(2, \max\left(\frac{f(r)}{r}, 1\right)\right). \tag{46}$$

When $1 < r$, $f(r)$ lies within the region B in Fig.6, that is, $1 < f(r) < 2$ and $f(r) < r$. And in the $\beta$ limiter form, it is

$$\phi = \max(0, 1, \min(r, \beta_2)) = \min(r, \beta_2), \quad \beta_2 = \min(2, \max(f(r), 1)). \tag{47}$$

By combining Eq.(46) and Eq.(47), the $\beta$ limiter form with $f(r)$ can be expressed as,

$$\phi = \max(0, \min(\beta_1 r, 1), \min(r, \beta_2)), \text{ with } \beta_1 = \min\left(2, \max\left(\frac{f(r)}{r}, 1\right)\right), \quad \beta_2 = \min(2, \max(f(r), 1)). \tag{48}$$

Thus, if the multi-dimensional limiting function is applied to Eq.(48), we obtain the multi-dimensional $\beta$ limiter form as

$$\phi = \max(0, \min(\beta_1 r, 1), \min(r, \beta_2)), \text{ with } \beta_1 = \min\left(\alpha, \max\left(\frac{f(r)}{r}, 1\right)\right), \quad \beta_2 = \min(\alpha, \max(f(r), 1)). \tag{49}$$

Exploiting Eq.(49), TVD limiters with the multi-dimensional limiting function can be derived as follows.

*MLP with minmod limiter:* $\phi = \max(0, \min(\beta_1 r, 1), \min(r, \beta_2)), \quad \beta_1 = \beta_2 = 1.$ (50a)

*MLP with van Leer limiter:* $\phi = \max[0, \min(\alpha, \alpha r, f(r))], \quad f(r) = \frac{2r}{1+r}.$ (50b)

*MLP with Superbee limiter:* $\phi = \max(0, \min(\alpha r, 1), \min(r, \alpha)).$ (50c)

*MLP with 3rd order interpolation (MLP3):* $\phi = \max[0, \min(\alpha, \alpha r, f(r))], \quad f(r) = \frac{1+2r}{3}.$ (50d)

*MLP with 5th order interpolation (MLP5):* $\phi = \max[0, \min(\alpha, \alpha r, f(r))],$ (50e)

where $f(r) = \frac{-2/r_{i-1}+11+24r_i-3r_ir_{i+1}}{30}.$

It is seen that in (50a), the multi-dimensional minmod limiter is exactly the same as the original minmod limiter of Eq.(6). It means that the original minmod limiter maintains monotonic property in multi-dimensional flows.

Figure 7 shows several limiting functions including minmod, van Leer, superbee limiter and 3rd order interpolation with TVD limiting. Those are the results without imposing the multi-dimensional effect, *i.e.*, $\alpha = 2$. Figure 8 is the region of MLP-van Leer, MLP-superbee limiter and MLP3. It is shown that MLP region is completely within the one-dimensional TVD limiting condition because the value of $\alpha$ is always between one and two.

Although $\alpha$ in the multi-dimensional limiting function is the complicated function of $r_L$, $r_R$, $\theta_{i or j}$ and $\theta_{i+1 or j+1}$, it can be roughly compared with TVD limiters by simplifying the property distribution as $1/r_R \approx r_L \approx r$ and $\theta_i \approx \theta_{i+1}$ on regular mesh. Then, the value of $\alpha$ becomes

When $0 < \frac{1}{r_R} < r_L < 1$,

$$1 < \alpha \approx \frac{2(1 + r\tan\theta)}{1 + \tan\theta} < 2 . \tag{51a}$$

When $\frac{1}{r_R} > r_L > 1$,

$$\alpha \approx \max\left(2, \frac{2r(1 + r\tan\theta)}{1 + \tan\theta}\right) = 2 . \tag{51b}$$

In discontinuous region of $(r << 1)$, when $\theta$ is zero, *i.e.*, the local one-dimensional assumption is readily acceptable, the value of $\alpha$ becomes two irrespective of $r$, which is identical to the range of superbee limiter. When $\theta \to 45^{\circ}$, the value of $\alpha$ becomes one, which is identical to the range of minmod limiter. As a result, the excessively steep slope based on one-dimensional flow assumption is restricted and oscillations across a multi-dimensional discontinuity are controlled. On the other hand, in discontinuous region of $(r >> 1)$, the value of $\alpha$ becomes two regardless of $\theta$ and $r$.

In smooth region, $r$ is nearly one, *i.e.*, $1/r_R \approx r_L \approx 1$ and $\alpha$ becomes nearly two regardless of $\theta$. Since $f(r) \approx 1$ $(r \approx 1)$, the limiter function reduces to

$$\phi \approx \max[0, \min(2, 2r, f)] = f . \tag{52}$$

This indicates that MLP3 and MLP5 can recover the fully 3rd and 5th order spatial accuracy in smooth region except for local extrema.

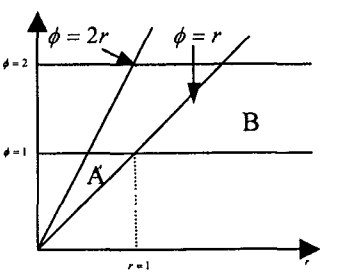


Fig. 6 TVD limiter region

## 4. NUMERICAL RESULTS

In order to investigate the actual performance of MLP, several test cases are carried out. Computed results by M-AUSMPW+[14] combined with MLP are compared with AUSMPW+ or Roe's FDS with TVD limiter. Furthermore, Roe's FDS with MLP and several TVD limiters are also compared. Since MLP is just an interpolation method independent of spatial discretization schemes, any numerical flux function can be essentially adopted. AF-ADI or LU-SGS is used for the time integration. Dual time stepping method or 3rd order TVD Runge-Kutta time integration [13] is used for unsteady calculation.
For boundary conditions, free stream values are specified as inflow conditions, and extrapolation from the inner computational domain is used for outflow condition. At wall, no-slip condition is specified for velocity, and adiabatic or constant condition is used for wall temperature.

### 4.1. Stationary vortex flow

It is relatively amenable to improve the accuracy of problems involving physical discontinuities only since the steeper variation always leads to the better result. On the other hand, in continuous flow, optimal variation is definitely necessary. To improve the accuracy of a vortex flow is one of the main objectives in the present paper since it is a good example of multi-dimensional continuous flows. If MLP is very prospective interpolation scheme both in discontinuous and continuous region, it should provide substantially enhanced results in vortex flows.

A vortex flow is a pure multi-dimensional phenomenon, characterized by the existence of negative pressure gradient toward core and the curved flow contours. A flow-aligned grid system is almost impossible in general cases and computed results are very sensitive to the choice of an interpolation and/or numerical fluxes. Figure 9 shows the typical computed result. It is Thomson-Rankine vortex model which is composed of the free vortex outside the core and the forced vortex inside.

a. free vortex (outside the core): $V_\theta \cdot r = const$ and $\frac{1}{\rho}\frac{\partial p}{\partial r} = \frac{V_\theta^2}{r}$.

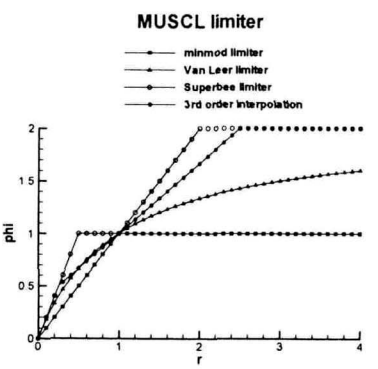


Fig.7 TVD limiters without multi-dimensional effect;

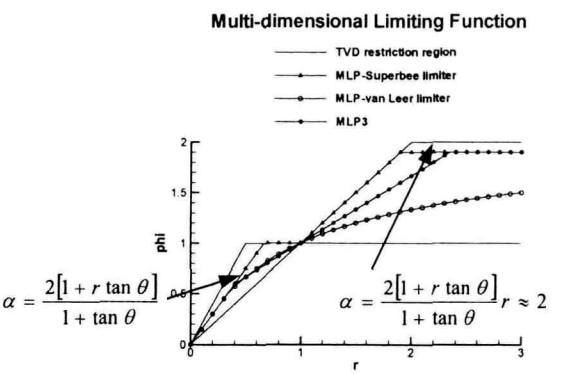


Fig.8 Comparison of several MLPs

b. forced vortex (inside the core): $V_\theta = \omega \cdot r$ and $\frac{dp}{dr} = \rho \frac{V_\theta^2}{r}$.

Angular velocity $\omega$ is 2 and core radius is 0.2. Maximum velocity is $0.36c_\infty$. Computational domain is from -2 to 2 with equal spacing. For grid convergence test, 25 by 25, 50 by 50, 75 by 75 and 100 by 100 grid points are employed. Roe's FDS, AUSMPW+ and M-AUSMPW+ are used for numerical fluxes and 3rd order TVD Runge-Kutta time integration method is used. CFL number is 0.8 and boundary is fixed as initial values. The pressure distributions are plotted at the non-dimensional time of 40.

Since viscous diffusion is not introduced, entropy is constant and a vortex flow should be maintained forever so long as centrifugal force is balanced with pressure gradient toward a vortex core. Thus, in the Euler equations, the ideal solution is the initial distribution itself.

Figures 10 and 11 show the results using van Leer limiter, MLP3 and MLP5. We can see the difference depending on interpolation schemes. Figures 12 and 13 show the accuracy improvement of MLP with M-AUSMPW+. It is shown that MLPs combined with M-AUSMPW+ can provide more accurate results than 3rd order interpolation scheme without limiting (see Eq.(11)). Figure 11 is the comparison of entropy variation according to interpolation schemes. In case of superbee, the vortex flow becomes stronger continuously meaning that entropy decreases without lower bound. As a result, it becomes unstable and after all, computation fails. As expected, MLP5 yields the least increase of entropy and it gives the best result among the interpolation schemes. This test case suggests that interpolation process should be compatible with flow physics.

Generally, interpolation step has been considered irrelevant to flow physics and treated mainly from the mathematical point of view. In actual computations, however, ideal approach is that all of the interpolation, spatial discretization and time integration schemes should follow flow physics faithfully. Among these, spatial discretization scheme is developed to satisfy the entropy condition. For example, AUSMPW+ and M-AUSMPW+ satisfy the entropy condition [19]. Entropy may decrease throughout time integration process, such as the redistribution of residual by an implicit scheme. Lastly, interpolation scheme definitely decreases entropy in some case as explained in Section 3.1.

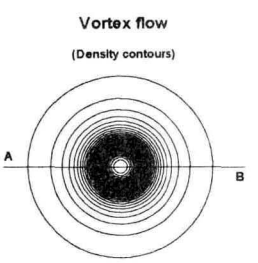


Fig. 9 Density contours of vortex flow;

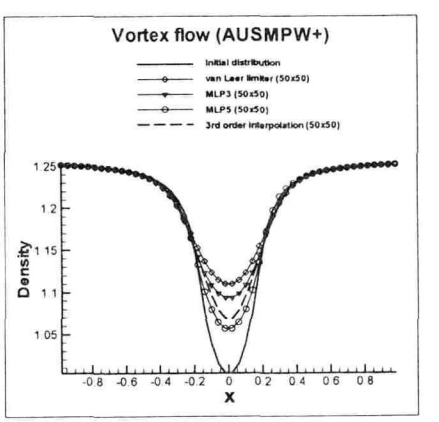


Fig. 10 Comparison of density distributions along the line AB

Figures 14 to 15 are the results of grid convergence test. Figure 15(a) shows the $L_1$ norm of density error when MLP3 is applied to AUSMPW+, Roe's FDS and M-AUSMPW+. As expected, due to slope limiting effect by the multi-dimensional limiting function, MLP3 is slightly less accurate than 3rd order interpolation scheme without limiting. As grid system becomes denser, MLP3 asymptotically approaches that 3rd order interpolation scheme. On the other hand, MLP3 with M-AUSMPW+ shows more accurate result than 3rd order interpolation with AUSMPW+ or Roe's FDS, *i.e.*, previous conventional upwind schemes.

Similarly, Fig. 15(b) show the $L_1$ norm of density error when MLP5 is applied to AUSMPW+, Roe's FDS and M-AUSMPW+. MLP5 is seen to provide accuracy between 3rd and 5th order spatial accuracy. Especially, MLP5 with M-AUSMPW+ is close to 5th order interpolation with AUSMPW+.

Based on the previous computations, MLP looks very promising in the computation of multi-dimensional flows including both discontinuous and continuous regions.

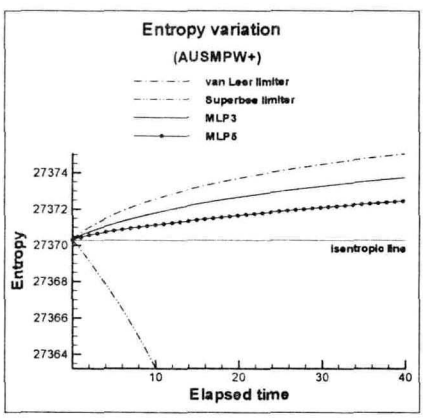


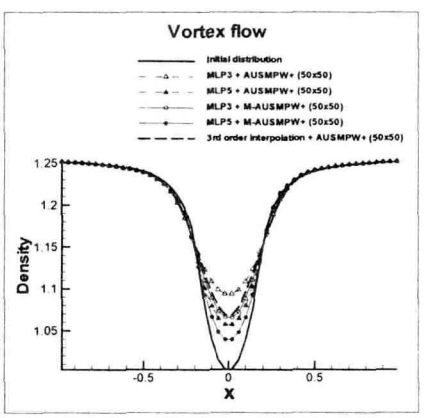


Fig. 11 Comparison of entropy variations of several interpolation schemes (left); Fig. 12 Comparison of density distributions of MLPs (right)

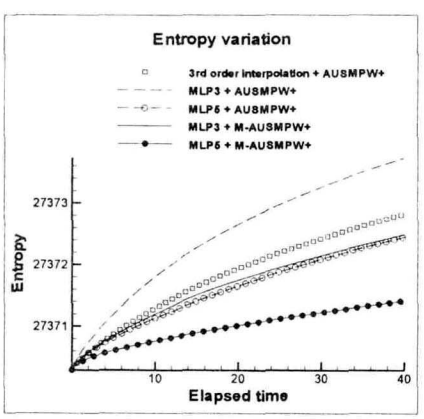


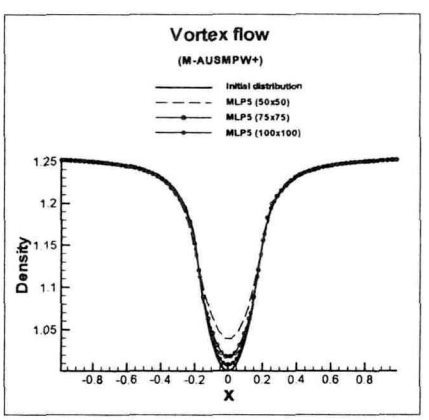


Fig. 13 Comparison of entropy variations (MLPs with AUSMPW+ and M-AUSMPW+) (left);
Fig. 14 Comparison of density distributions along the line AB (right)

### 4.2. Double shock reflection

The free stream Mach number is two and the deflection angle of the lower wall is 15 degree angle. The grid system is 100 by 30. Slip boundary condition is applied on the upper and lower walls, and all physical values at the exit are extrapolated. This test problem shows the advantages of MLP clearly in terms of monotonicity and convergence.

Figures 16 are the comparisons of pressure distribution of superbee, MLP-superbee limiters, MLP3 and MLP5. The original superbee limiters exhibits pressure oscillations across the oblique shock and does not maintain a monotonic profile as shown in Figs. 17 and 18. The result by van Leer limiter also shows similar overshoot phenomenon. On the other hand, MLP-superbee limiter provides the best result in maintaining a monotonic shock distribution. MLP3 and MLP5 also do not show overshoot phenomenon and yield almost the same accuracy as MLP-superbee limiter. At a glance, MLP-superbee limiter gives the best monotonic result across physical discontinuities. However, it shares the same defect of the

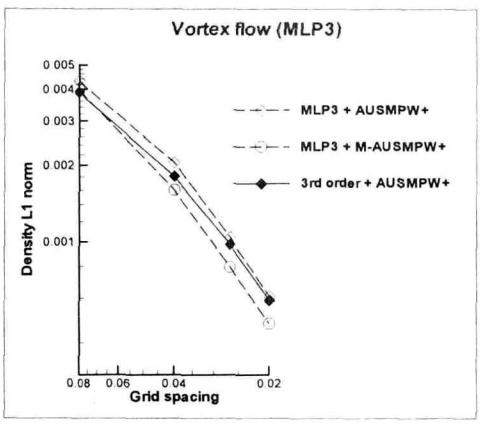


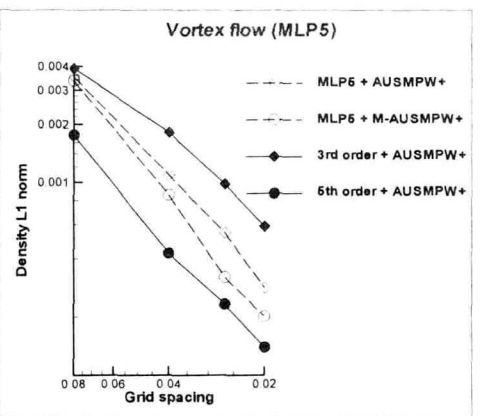


Fig. 15(a) Grid convergence of MLP3 (AUSMPW+ and M-AUSMPW+) (left); Fig. 15(b) Grid convergence of MLP5 (AUSMPW+ and M-AUSMPW+) (right)

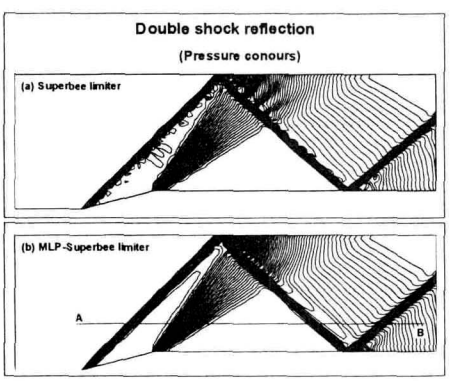


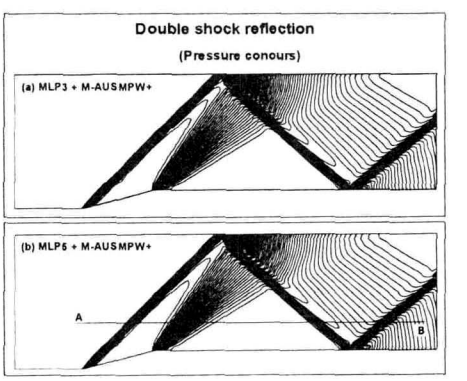


Fig. 16(a) Comparison of pressure contours (superbee and MLP-superbee limiters) (left); Fig. 16(b) Comparison of pressure contours (MLP3 and MLP5) (right)

original superbee limiter in a sense that entropy decreases in a continuous expansion flow, which is examined in the next test case.

Figure 19 shows the error history. CFL number is 3.0 and LU-SGS is used for time integration. Even if the test case is simple, superbee and van Leer limiters are never converged due to oscillatory behavior across the oblique shock discontinuity. On the other hand, MLP-superbee limiter, MLP3 and MLP5 show good convergence characteristics.

### 4.3. Viscous shock tube problem

The viscous shock tube problem [20,21] is revisited to examine the accuracy of MLP in complex shock viscous flows. The Reynolds number is 200 with constant viscosity and the initial state is $(\rho,u,v,p)_L = (120,0,0,120/\gamma)$ and $(\rho,u,v,p)_R = (1.2,0,0,1.2/\gamma)$. Viscous fluxes are calculated by 4th order spatial accuracy, and 3rd order TVD Runge-Kutta method is used.

Figure 20 is the comparison of density contours. Case(a) to (c) are results by van Leer limiter with AUSMPW+ on coarse (250 x 125), medium (350 x 175) and fine (500 x 250) grid system, and case(d) to (f) are results by MLP5 with M-AUSMPW+ on the same grid

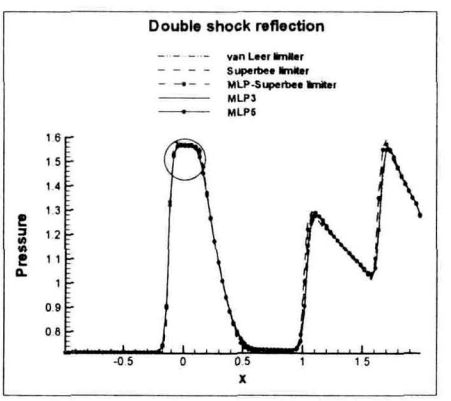


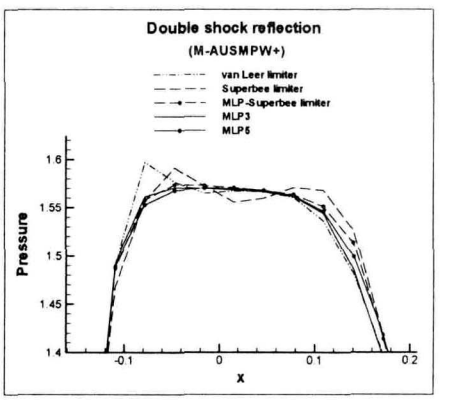


Fig.17 Comparison of pressure distributions along the line AB (left); Fig. 18 Comparison of pressure distributions in circle region (right)

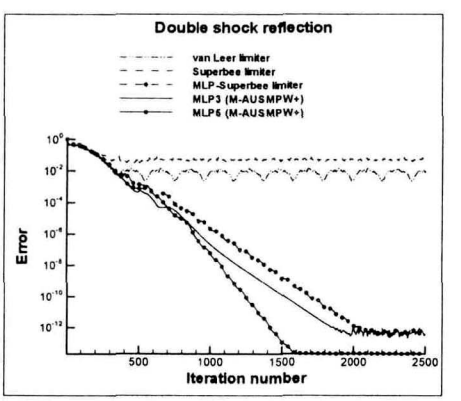


Fig.19 Error history of double shock reflection

systems. MLP5 with M-AUSMPW+ on coarse grid system shows a much better result than van Leer limiter with AUSMPW+ on medium grid system, which has twice more grid points. Furthermore, it is very similar to the fine grid result which has four times more grid points. MLP on medium grid system also shows a better result than van Leer limiter with AUSMPW+ on fine grid system, and almost reaches the grid converged result (MLP on fine grid system).

Judging from the direct comparison, MLP5 with M-AUSMPW+ can give about three times grid point reduction effect. If the influence of iteration number is included, actual grid reduction effect increases even further. When the same scheme is used, iteration number is generally proportional to grid size in unsteady flow calculations. For that reason, the total iteration number for case(c) and case(f) are almost double compared to case(a) and case(d). Thus, it may say that MLP5 with M-AUSMPW+ saves the total computational cost about six times in providing the same level of accuracy. Comparison with other interpolation schemes such as WENO or ACM can be referred to Ref.[24].

Table 1 is the comparison of the primary vortex size. The height and angle of the primary vortex, which is sensitive to numerical dissipation, is converged to 0.168. Even on fine grid system, van Leer limiter with AUSMPW+ yields smaller vortex while MLP5 with M-AUSMPW+ on medium grid system gives the identical results in terms of vortex height and angle. Comparing vortex size, case(d) to case (f) provide about four times grid point reduction effect over case(a) to case (c).

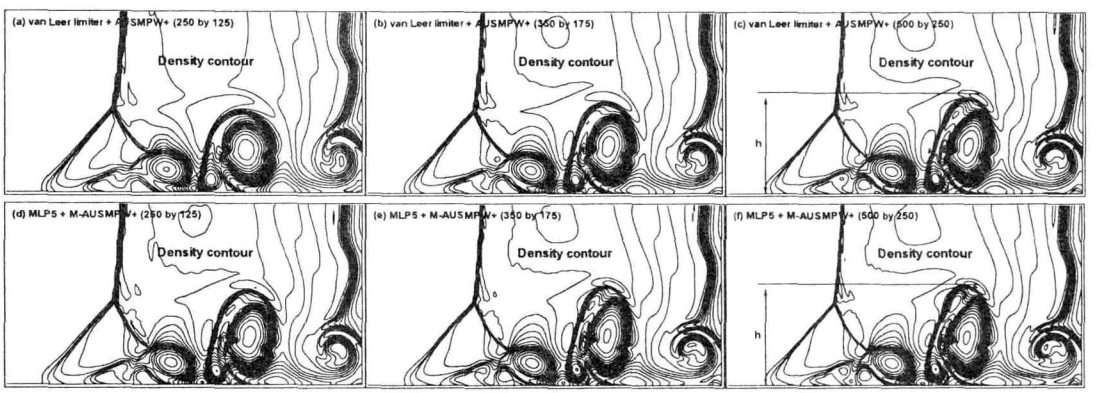


Fig. 20 Density distributions according to grid points and numerical schemes

Table 1. Comparison of the height of the primary vortex

| Scheme | Case(a) (250by125) | Case(b) (350by175) | Case(c) (500by250) | Case(d) (250by125) | Case(e) (350by175) | Case(f) (500by250) |
|---|---|---|---|---|---|---|
| Height (h) | 0.142 | 0.155 | 0.163 | 0.161 | 0.168 | 0.168 |

## 5. CONCLUSIONS

By analyzing conventional TVD limiters and exploiting higher order TVD interpolation based on the information on local curvature distribution, a new multi-dimensional limiting function is derived. And, a new Multi-dimensional Limiting Process (MLP) is developed by combining the multi-dimensional limiting function with a higher order polynomial interpolation. The newly developed method turns out to have several desirable characteristics such as multi-dimensional monotonicity across a discontinuity, robust convergence and computational efficiency comparable to conventional TVD limiters. In addition, higher order interpolation can be easily incorporated.

The most distinguishable property of MLP is to provide non-oscillatory profiles in multi-dimensional flows and, as a result, a good convergence characteristic. Thanks to the properties, MLP combined with M-AUSMPW+ can significantly increase accuracy, convergence/robustness and efficiency both in steady and unsteady multi-dimensional flows containing physical discontinuities. Through numerous test cases including a vortex flow, a shock-wave/boundary-layer interaction, shock wave/vortex interaction and viscous shock tube problem, it is verified that MLP can control numerical oscillations in multi-space dimensions. In addition to robustness improvement across a discontinuity, accuracy enhancement in pure multi-dimensional problems such as separated flows or vortex flows is remarkable, especially combined with M-AUSMPW+. From the numerous computed results, MLP with M-AUSMPW+ generally provides three or four times accuracy improvement in terms of grid points, compared with TVD with popular flux functions. Also, it does not show the entropy decreasing phenomenon in an expansion flow region.

Through the extension of current outcomes to three-dimensional flows, MLP is expected to bring substantial reduction of computational cost and accuracy improvement simultaneously.

## ACKNOWLEDGEMENT

The authors appreciate financial support by the Korea Science and Engineering Foundation (Grant R01-2005-000-10059-0).

## REFERENCES

[1] **P. L. Roe.** *Discrete Models for the Numerical Analysis of Time-Dependent Multidimensional Gas Dynamics*, Journal of Computational Physics, Vol.63, 1986.

[2] **C. Rumsey** *Development of a Grid-Independent Approximate Riemann Solver*, Ph. D. Thesis, University of Michigan, 1991.

[3] **C. Lacor and Ch. Hirsch** *Genuinely Upwind Algorithms for Multidimensional Euler Equations*, AIAA Journal, Vol 30(1), 1991.

[4] **Dadone, and B. Grossman** *Characteristic-Based, Rotated Upwind Scheme for the Euler Equation*, AIAA Journal 30(9), 1992.

[5] **D. W. Levy, K. G. Powell, and B. Van Leer** *Use of a Rotated Riemann Solver for the Two-Dimensional Euler Equations*, Journal of Computational Physics, 106, 201-214,

1993.

[6] **D. Sidilkover** *A Genuinely Multidimensional Upwind Schemes and Efficient Multigrid Solver for the Compressible Euler Equations*, Submitted the Journal of Computational Physics.

[7] **H. Deconinck, H. Paillere, R. Struijs, and P. L. Roe** *Multidimensional Upwind Schemes Based on Fluctuation-splitting for Systems of Conservation Laws*, Computational Mechanics, 13, 323-340, 1993.

[8] **Y. Tamura, and K. Fuji** *A Multi-Dimensional Upwind Scheme for the Euler Equations on Structured Grids*, Computers and Fluids, 22(2/3), 125-137, 1993.

[9] **A. Harten** *High Resolution Schemes for Hyperbolic Conservation Law*, Journal of Computational Physics, 49(3), 357-393, 1983.

[10] **P. K. Sweby** *High Resolution Schemes Using Flux Limiters for Hyperbolic Conservation Laws*, SIAM Journal on Numerical Analysis, 21(5), 995-1011, 1984.

[11] **A. Harten, B. Enquist, S. Osher, and S. R. Chakravarthy** *Uniformly High Order Accurate Essentially Non-oscillatory Schemes, III*, Journal of Computational Physics, 71(2), 231-303, 1987.

[12] **C. W. Shu** *TVB Uniformly High-Order Schemes for Conservation Laws*, Mathematics of Computation, 49(179), 105-121, 1987.

[13] **C. W. Shu and S. Osher** *Efficient Implementation of Essentially Non-oscillatory Shock-capturing Schemes*, Journal of Computational Physics, 77, 439-471, 1988.

[14] **K. L. Lee, S. H. Yoon, C. Kim and K. H. Kim** *Accurate and Efficient Re-evaluation of Cell-interface Convective Fluxes*, Journal of the KSIAM, submitted.

[15] **B. van Leer** *Toward the ultimate conservative difference scheme*, Journal of Computational Physics, 32, 101 – 136, 1979.

[16] **A. Jameson** *Analysis and Design of Numerical Schemes for Gas Dynamics 1 Artificial Diffusion, Upwind Biasing, Limiters and Their Effect on Accuracy and Multigrid Convergence*, International Journal of Computational Fluid Dynamics, 4, 171-218, 1995.

[17] **J. B. Goodman and R. J. LeVeque** *On the Accuracy of Stable Schemes for 2D Scalar Conservation laws*, Mathematics of Computation, 45, 15-21, 1985.

[18] **S. P. Spekreijse** *Multigrid solution of monotone second-order discretizations of hypersonic conservations laws*, Mathematics of Computation, 49, 135-155, 1987.

[19] **K. H. Kim, C. Kim and O. H. Rho** *Methods for the Accurate Computations of Hypersonic Flows, Part I: AUSMPW+ Scheme*, Journal Computational Physics, 174, 38-80, 2001.

[20] **V. Daru, C. Tenaud** *Evaluation of TVD high resolution schemes for unsteady viscous shocked flows*, Computers and Fluids, 30, 89-113, 2001.

[21] **B. Sjögreen, H. C. Yee** *Grid convergence of high order methods for multiscale complex unsteady viscous compressible flows*, Journal of Computational Physics, 185, 1-26, 2003.

Heeseok Koo
2004 B.S. Mechanical and Aerospace Engineering, Seoul National University

Sung-Hwan Yoon
2003 B.S. Mechanical and Aerospace Engineering, Seoul National University
2005 M.S. Mechanical and Aerospace Engineering, Seoul National University

Chongam Kim
E-mail : chongam@snu.ac.kr
1988 B.S. Aerospace Engineering, Seoul National University
1990 M.S. Aerospace Engineering, Seoul National University
1997 Ph.D Mechanical and Aerospace Engineering, Princeton University
1997~1998 Stanford University Center for Turbulence Research / Research Fellow
1998~1999 Instructor, Dept. of Mechanical and Aerospace Engineering, Seoul National University
2000~2004 Assistant Professor, Dept. of Mechanical and Aerospace Engineering, Seoul National University
2004~present Associate Professor, Dept. of Mechanical and Aerospace Engineering, Seoul National University
Research Field : Numerical method for computational physics
Application of gaskinetic schemes in CFD
Hypersonic and high temperature gas dynamics
Aerodynamic shape optimization and flow control
Unstructured based flow solver and mesh generation

Kyu-Hong Kim
E-mail : aerocfd1@snu.ac.kr
1994 B.S. Aerospace Engineering, Seoul National University
1997 M.S. Aerospace Engineering, Seoul National University
2001 Ph.D Mechanical and Aerospace Engineering, Seoul National University
2004~present Assistant Professor, Dept. of Mechanical and Aerospace Engineering, Seoul National University
Research Field : Numerical algorithm development for non-equilibrium hypersonic flows
Reentry aerodynamics including non-equilibrium reactive gas, rarified gas, radiation
High temperature magneto-hydrodynamics